ASTFE American Society of Thermal and Fluids Engineers

5th Thermal and Fluids Engineering Conference (TFEC)
April 5–8, 2020
New Orleans, LA, USA

TFEC-2020-32440

A ROBUST ANALYTIC MODEL OF FOLDED FIN COLD PLATES FOR AUTOMOTIVE POWER ELECTRONICS COOLING

Andrew J. Bomar*[1], Thomas M. Adams[2]

[1]University of Central Florida, Orlando, FL, 32816, USA
[2]Rose-Hulman Institute of Technology, Terre Haute, IN, 47803, USA

ABSTRACT

The development of high power density automotive power electronics led to newer, and often more costly, cooling solutions in pursuit of maintaining desirable operating temperatures. This has been followed by a shift of focus from proving new technologies to producing low-cost electric and hybrid-electric vehicles accessible to more customers, resulting in renewed interest in low-cost solutions to power electronics cooling. Folded fins are one such solution, common on mass produced heat exchangers, and have been applied in legacy power electronics cooling systems. This paper presents an analytic model that allows for an expedient, robust, and accurate thermal analysis of a folded fin cold plate. The model combines empirical and algebraic approaches to capture heat transfer effects in a 3-dimensional, multi-phase domain including the transistor, cold plate, and coolant. In practice, computational analysis is often used in place of empirical and mathematical methods. The methods described here have the advantages of allowing for broader and more efficient trade studies due to vastly shorter solution times and providing junction temperature estimates within 5 °C of computational methods, and therefore complement computational methods. Lastly, use of the model to design a cold plate for an insulated-gate bipolar transistor cooling system in a hybrid electric vehicle is described. The model is used to explore manufacturability constraints, fouling criteria, assembly methods, fin types, and materials of construction. The result is a design that provides a comparable operating junction temperature in the IGBTs with a significant cost reduction compared to a more exotic legacy design.

KEY WORDS: Cold Plate, Power Electronics Cooling, Analytic Modeling, Folded Fin

1. INTRODUCTION

Insulated gate bipolar transistors (IGBTs) are a type of high-current transistor commonly used in power electronics, with applications ranging from wind turbines to hybrid-electric vehicles (HEVs) and full electric vehicles (EVs). The high-power applications of IGBTs lead to high levels of heat generation within the devices. As a result, dedicated systems for IGBT cooling are common. In automotive applications, such cooling is often provided indirectly via liquid engine coolant. A representative architecture of an IGBT cooling system in an automotive power electronics application is detailed in Fig. 1.

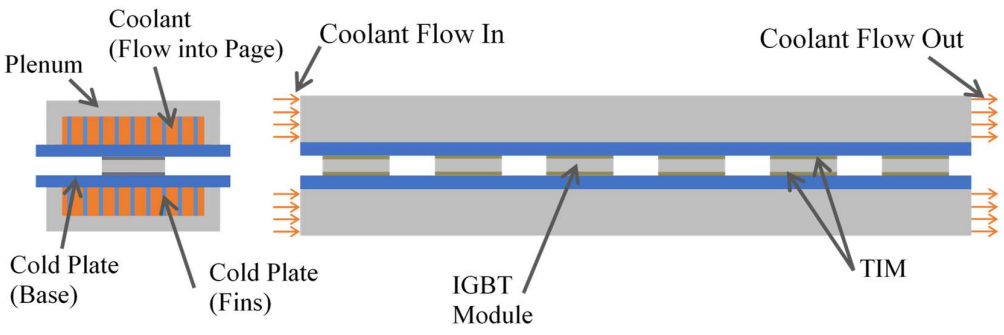

Fig. 1 Schematic diagram of an IGBT cooling system: front view (left), side view (right).

*Corresponding Author: abomar@knights.ucf.edu

The architecture in Fig. 1 is from a developmental power electronics module for HEV applications. The system uses a 50%-50% mixture of ethylene glycol and water as coolant. Each IGBT is packaged with other devices into a single module. A diode is included in this package and is of significance because it is a second source of heat generation within the IGBT module. Six IGBTs are arranged in a row and are clamped between two cold plates with parallel coolant flow. A thermal-interface material (TIM) is used between the cold plates and the IGBT packages. For each cold plate, a plenum fits snuggly over the fins and seals to the base. Coolant is passed through the plenum, which forces the coolant through the channels formed between the fins.

The present work seeks to develop an analytic model to aid in the comparison of a folded fin design to other cold plate designs for indirect liquid IGBT cooling systems. The geometric complexity of the cold plate has resulted in computational fluid dynamics (CFD) models, which require hours of processing time, being a preferred approach for analysis. A combined empirical and algebraic approach complements CFD by offering a time-efficient alternative for industry trade studies and a robust tool for CFD result validation throughout detailed industry or academic design analysis.

Folded fins are common on mass produced heat exchangers, such as automotive radiators and microchannel condensers for air-conditioners. Folded fins have also been applied in power electronics cooling systems, but many other options have been explored for thermodynamic improvements. Renewed interest in indirect cooling with cold plate designs that are cost-effective in mass production can be expected as EV and HEV production volumes are increasing. A secondary goal of this work was to demonstrate the potential of folded fins for use in a specific HEV power electronic cooling application.

2. GEOMETRIC PARAMETERS

2.1 Folded Fin Geometry

The three types of folded fins discussed here are straight (i.e. plain), wavy (i.e. ruffled), and lanced (i.e. offset). These fin types are available from most folded fin manufacturers. Many more complex fin types are also available. The louvers and other complex features of those fin types can be prone to fouling and therefore were not included in this investigation. However, the model presented would still be applicable, presuming that empirical correlations are available that describe flow through the intended folded fin geometry.

Fig. 2 shows the geometric parameters of folded fins, as defined for this model. For lanced and wavy folded fins, additional parameters are necessary to fully specify the shape.

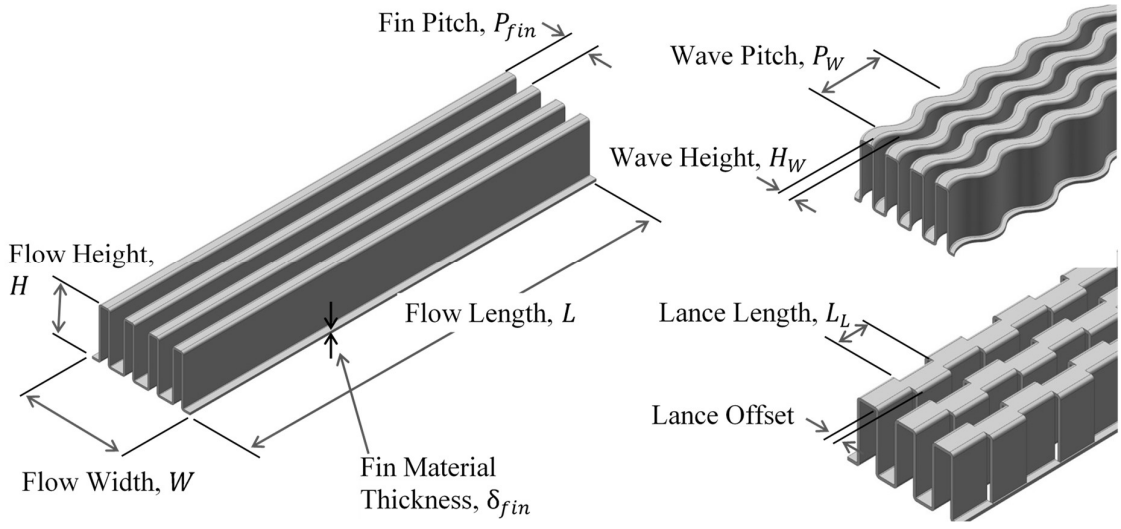

Fig. 2 Schematic of folded fin geometric parameters.

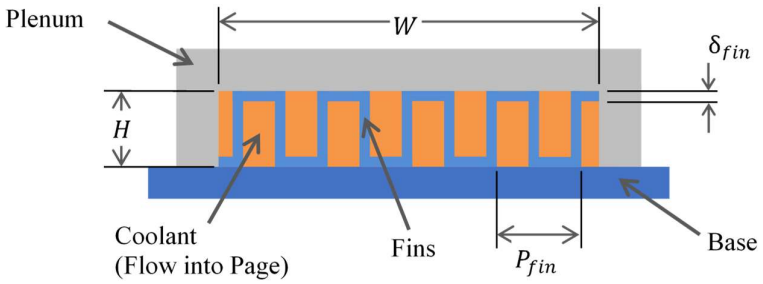

Fig. 3 Schematic of channel flow geometry.

2.2 Flow Channel Geometry

Coolant flowing into the plenum is divided into separate channels, as shown in Fig. 3. This flow was modeled with various analytic and empiric relationships. Equations 1 – 4 are relations used to calculate important dimensions of these cross-sections. A_{chan} is the cross-sectional area of one channel, D_h is the hydraulic diameter, α is the aspect ratio of the channel, and β is the blocking ratio of the fins.

$$A_{chan} = \left(H - \delta_{fin}\right)\left(\frac{P_{fin}}{2} - \delta_{fin}\right) \tag{1}$$

$$D_h = \frac{4A_{chan}}{2\left(H + \frac{P_{fin}}{2} - 2\delta_{\text{fin}}\right)} \tag{2}$$

$$\alpha = \frac{\frac{P_{fin}}{2} - \delta_{\text{fin}}}{H - \delta_{\text{fin}}} \tag{3}$$

$$\beta = \frac{P_{fin}H - 2\left(\frac{P_{fin}}{2} - \delta_{fin}\right)\left(H - \delta_{fin}\right)}{P_{fin}H} \tag{4}$$

If the partial channels on either side of the fin array are assumed to be equivalent to one whole channel, then the number of fins, N, is also equal to the number of channels. This relation is shown in Equation 5, with the floor function indicating that the value is rounded down. The total open cross-sectional area for flow through the channels, $A_{chan,tot}$, is then calculated as shown in Equation 6.

$$N = \left\lfloor \frac{W}{P_{fin}/_2} \right\rfloor \tag{5}$$

$$A_{chan,tot} = W \cdot H - N \cdot \delta_{fin} \cdot \left(H + \frac{P_{fin}}{2} - \delta_{fin}\right) \tag{6}$$

Additional parameters are defined for the wavy fin type to capture the effects of the increased flow length due to the serpentine shape of the channels. The wavy fin corrugation ratio, γ is defined in Equation 7. The path length of a period of a sinusoidal channel, s_W, is calculated with Equation 8, with the function E representing the complete elliptic integral of the second kind. (Awad and Muzychka, 2011)

$$\gamma = \frac{H_W}{P_W} \tag{7}$$

$$s_W = 2P_W \frac{\sqrt{1+\gamma^2\pi^2}}{\pi} \mathrm{E}\left(\frac{\gamma\pi}{\sqrt{1+\gamma^2\pi^2}}\right) \tag{8}$$

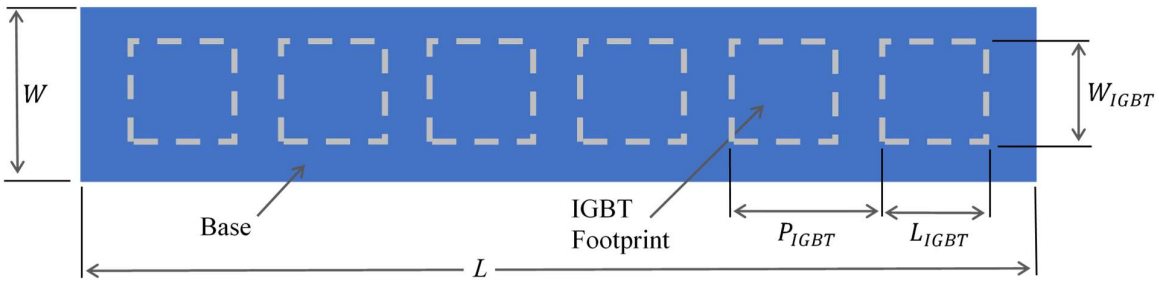

Fig. 4 Folded fin cold plate base geometry.

For the lanced fin design, the correlations presented use an alternate definition for the hydraulic diameter, $D_{h,L}$, defined with Equation 9. The lance offset dimension from Fig. 2 is not used in this model. (Kim et al., 2011)

$$D_{h,L} = \frac{4\left(\frac{P_{fin}}{2} - \delta_{fin}\right)\left(H - \delta_{fin}\right)L_L}{2\left[\left(\frac{P_{fin}}{2} - \delta_{fin}\right)L_L + \left(H - \delta_{fin}\right)L_L + \delta_{fin}\left(H - \delta_{fin}\right)\right] + \delta_{fin}\left(\frac{P_{fin}}{2} - \delta_{fin}\right)} \quad (9)$$

2.3 Cold Plate and IGBT Footprint Geometry

The cold plate consists of a folded fin array joined to a base. The relevant dimensions of the base, including the footprints of the IGBTs on the underside, are shown in Fig. 4. P_{IGBT} is the pitch, or spacing, of the row of IGBTs and is assumed to be uniform. The thickness of the base, δ_{base}, is the dimension into the page.

3. EMPIRICAL FLOW PARAMETERS

3.1 Reynolds Number Calculation

Average velocity of the coolant flowing through the plenum is given as Equation 10, where $\dot{V}$ is the volumetric flow rate. Reynolds number for the flow inside of each channel of the cold plate is given as Equation 11.

$$u_{avg} = \frac{\dot{V}}{A_{chan,tot}} \quad (10)$$

$$\mathrm{Re} = \frac{\rho u_{avg} D_h}{\mu} \quad (11)$$

3.2 Straight Fin Empirical Flow Parameters

In absence of disruptions to flow (such as wavy or lanced fins), a Reynolds number less than 2300 generally implies laminar flow. In this flow domain, the approach used to calculate Darcy friction factor, f, and the Nusselt number at constant heat flux, Nu, are polynomial regressions fitted to exact solutions to the differential momentum and energy equations based on the aspect ratio of rectangular channels (Shah and London, 1978).

$$\mathrm{fRe} = 96(1 - 1.3353\alpha + 1.9467\alpha^2 - 1.7012\alpha^3 + 0.9564\alpha^4 - 0.2537\alpha^5) \quad \mathrm{Re} \leq 2300 \quad (12)$$

$$\mathrm{Nu} = 8.325(1 - 1.3353\alpha + 1.9467\alpha^2 - 1.7012\alpha^3 + 0.9564\alpha^4 - 0.2537\alpha^5) \quad \mathrm{Re} \leq 2300 \quad (13)$$

Internal flows well above 2300 can be considered fully turbulent. For this analysis, any flow with Reynolds number above 3000 was treated with empirical relations for turbulent flow. Friction factor was calculated with Equation 14 from Petukhov (1970), which is considered valid for $3000 \lesssim \mathrm{Re} \lesssim 500{,}000$. This equation requires the assumption of smooth channels. The empirical correlation used for the Nusselt number is given in Equation 15 from Gnielinksi (1976), is also valid for $3000 \lesssim \mathrm{Re} \lesssim 500{,}000$, and valid for $0.5 \lesssim \mathrm{Pr} \lesssim 2000$.

$$\mathrm{f} = [0.79\ln(\mathrm{Re}) - 1.64]^{-2} \quad \mathrm{Re} \geq 3000 \quad (14)$$

$$\mathrm{Nu} = \frac{\frac{\mathrm{f}}{8}(\mathrm{Re} - 1000)\mathrm{Pr}}{1 + 12.7\left(\frac{\mathrm{f}}{8}\right)^{0.5}\left(\mathrm{Pr}^{2/3} - 1\right)} \quad \mathrm{Re} \geq 3000 \tag{15}$$

To create continuous equations for f and Nu, if the value of the Reynolds number falls between 2300 and 3000 an interpolation is performed between the solutions at Re = 2300 and Re = 3000.

3.3 Wavy Fin Empirical Flow Parameters

As highlighted in a review from Sheik Ismail et al. (2010), a body of experimental data exists for flow and heat transfer in wavy channels but development of robust empirical correlations has been limited. Recent reviews by Aliabadi (2014) and Kurtulmus and Sahin (2019) haven't revealed significant changes to this position. Sparrow and Hossfeld (1984) presented simple correlations based on experimental data but Gradeck et al. (2005) reported errors in Nusselt number over 100% when applied to other heat exchangers. Junqi et al. (2007) published correlations based on more extensive experiments but they are specific to air-cooled heat exchangers.

The most robust correlation to date is likely found in the work from Awad and Muzychka (2011). They proposed that the friction factor and Nusselt number asymptotically approach the conditions of a straight channel at low Reynolds number and approach the conditions in the laminar boundary layer of external flow at high Reynolds number. RMS error of the predicted friction factor and Colburn factor, j, was typically within 25% of data from four other studies of heat exchangers with varied geometry and Prandtl number, with a maximum RMS error of 50% when compared to the data from Junqi et al. (2007).

At the limit of low Reynolds number, the friction factor in a wavy channel, f_W is assumed to be equivalent to the value for f as calculated in Equation 12 with a correction for the increased path length due to the wavy channel, as shown in Equation 16. The Nusselt number, Nu_W, at the limit of low Reynolds number is assumed to be equivalent to the value for from Equation 13, with the correction for increased path length and heat transfer surface area as shown in Equation 31. (Awad and Muzychka, 2011)

$$\mathrm{f}_W = \mathrm{f}_{equation\ 12}\frac{s_W}{P_W} \tag{16}$$

$$\mathrm{Nu}_W = \mathrm{Nu}_{equation\ 13} \tag{17}$$

At the limit of high Reynolds number, the value of the friction factor is assumed to equal the value of the apparent friction factor at the entrance to a channel, $\mathrm{f}_{\mathrm{app}}$. A dimensionless length, L^+ is defined in Equation 18 and Equation 19 is valid for values of $L^+ < 0.001$. Some of the geometries analyzed in this work violated this limit from the original work by Shapiro et al. (1954), but Awad and Muzychka (2011) do not address this limitation. The Nusselt number at the limit of high Reynolds number, Nu_{LBL} is estimated with a correlation for the Nusselt number in the laminal boundary layer (Awad and Muzychka, 2011).

$$L^+ = \frac{s_W}{2D_h\mathrm{Re}} \tag{18}$$

$$\mathrm{f}_{app} = \frac{3.44}{\sqrt{L^+}} \quad L^+ < 0.001 \tag{19}$$

$$\mathrm{Nu}_{LBL} = 0.664\left(\mathrm{Re}\frac{s_W}{2D_h}\right)^{1/2}\mathrm{Pr}^{1/3} \tag{20}$$

The values for Darcy friction factor, f, and the Nusselt number at constant heat flux, Nu, in the wavy channel are then calculated with Equations 21 and 22. The power values of 2 and 5 in these equations, respectively, were determined by Awad and Muzychka (2011) to provide the best fit to the available experimental data.

$$f = \left(f_W{}^2 + f_{app}{}^2\right)^{1/2} \tag{21}$$

$$Nu = \left(Nu_W{}^5 + Nu_{LBL}{}^5\right)^{1/5} \tag{22}$$

3.4 Lanced Fin Empirical Flow Parameters

Several studies present correlations for lanced folded fins (Joshi and Webb, 1987; Manglik and Bergles, 1995). Kim et al. (2011) present correlations built on previous works but are valid for fluids with varied Pr. An alternate Reynolds number, Re_L, is calculated with the altered $D_{h,L}$ from Equation 9. The piecewise relations for f and j are then given below as Equations 23 and 24. Nusselt number is related to the Colburn factor as in Equation 25.

$$f = \begin{cases} e^{7.91}\alpha^{-0.159}\left(\frac{\delta_{fin}}{L_L}\right)^{0.358}\left(\frac{\delta_{fin}}{\frac{P_{fin}}{2}-\delta_{fin}}\right)^{-0.033} Re_L{}^{(0.126\ln(Re_L)-2.3)} & \beta < 0.2 \\ e^{9.36}\alpha^{-0.0025}\left(\frac{\delta_{fin}}{L_L}\right)^{-0.0373}\left(\frac{\delta_{fin}}{\frac{P_{fin}}{2}-\delta_{fin}}\right)^{1.85} Re_L{}^{(0.142\ln(Re_L)-2.39)} & 0.2 \leq \beta < 0.25 \\ e^{5.58}\alpha^{-0.36}\left(\frac{\delta_{fin}}{L_L}\right)^{0.552}\left(\frac{\delta_{fin}}{\frac{P_{fin}}{2}-\delta_{fin}}\right)^{-0.521} Re_L{}^{(0.111\ln(Re_L)-1.87)} & 0.25 \leq \beta < 0.3 \\ e^{4.84}\alpha^{-0.48}\left(\frac{\delta_{fin}}{L_L}\right)^{0.347}\left(\frac{\delta_{fin}}{\frac{P_{fin}}{2}-\delta_{fin}}\right)^{0.511} Re_L{}^{(0.089\ln(Re_L)-1.49)} & 0.3 \leq \beta < 0.35 \end{cases} \tag{23}$$

$$j = \begin{cases} e^{1.96}\alpha^{-0.098}\left(\frac{\delta_{fin}}{L_L}\right)^{0.235}\left(\frac{\delta_{fin}}{\frac{P_{fin}}{2}-\delta_{fin}}\right)^{-0.154} Re_L{}^{(0.0634\ln(Re_L)-1.3)} Pr^{0.00348} & \beta < 0.2 \\ 1.06\alpha^{-0.1}\left(\frac{\delta_{fin}}{L_L}\right)^{0.131}\left(\frac{\delta_{fin}}{\frac{P_{fin}}{2}-\delta_{fin}}\right)^{-0.08} Re_L{}^{(0.0323\ln(Re_L)-0.856)} Pr^{0.0532} & 0.2 \leq \beta < 0.25 \\ e^{1.3}\alpha^{0.004}\left(\frac{\delta_{fin}}{L_L}\right)^{0.251}\left(\frac{\delta_{fin}}{\frac{P_{fin}}{2}-\delta_{fin}}\right)^{0.031} Re_L{}^{(0.0507\ln(Re_L)-1.07)} Pr^{0.051} & 0.25 \leq \beta < 0.3 \\ 0.2\alpha^{-0.125}\left(\frac{\delta_{fin}}{L_L}\right)^{0.21}\left(\frac{\delta_{fin}}{\frac{P_{fin}}{2}-\delta_{fin}}\right)^{-0.069} Re_L{}^{(0.0005\ln(Re_L)-0.338)} Pr^{0.0549} & 0.3 \leq \beta < 0.35 \end{cases} \tag{24}$$

$$Nu = jRe_L Pr^{1/3} \tag{25}$$

3.5 Pressure Loss and Heat Transfer Coefficient

Equation 26 is used to calculate the coolant pressure loss, Δp. Equation 27 was used to calculate h, the average convective heat transfer coefficient inside of the channels.

$$\Delta p = \frac{fL\rho u_{avg}{}^2}{2D_h} \tag{26}$$

$$h = \frac{k\mathrm{Nu}}{D_h} \tag{27}$$

4. COLD PLATE THERMAL RESISTANCE MODEL

A thermal resistance circuit of the domain of the cold plate model is shown in Fig. 5 . Heat transfer occurs through the IGBT package and TIM, with 3-dimensional spreading inside the base, and through three paths between the base of the cold plate and the center of the working fluid.

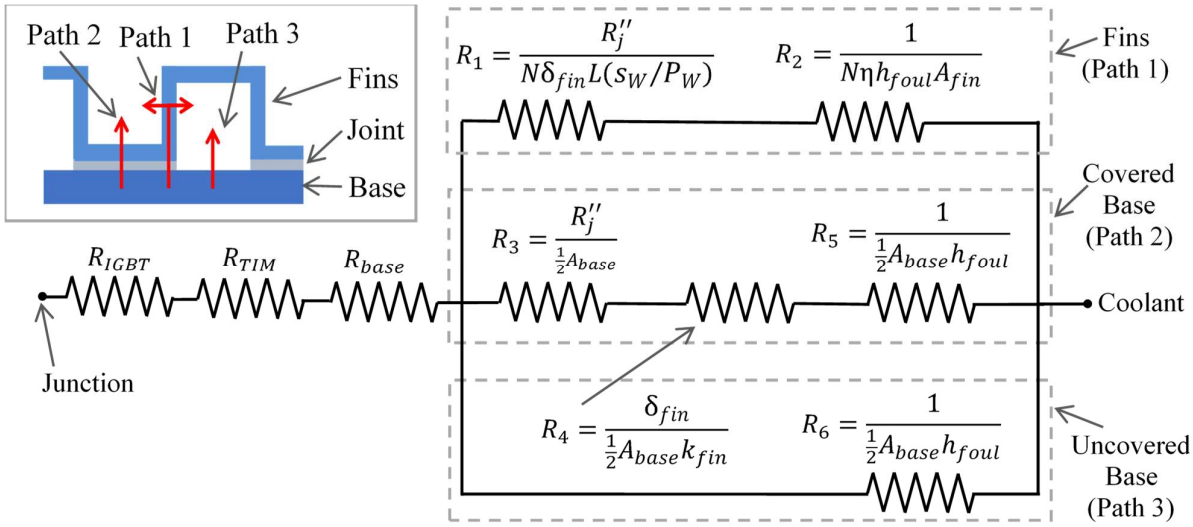

Fig. 5 Thermal resistance circuit of the fluid and solid model domains.

4.1 Fouling Factor

A fouling factor, R''_{foul}, is commonly included in heat exchanger models as a surface thermal resistance in series with other thermal resistances. In this model, the fouling factor is incorporated through a modified heat transfer coefficient, h_{foul}, in order to account for fouling in the fin efficiency relation used, Equation 32. Equation 28 demonstrates contributions to the surface thermal resistance due to convection and due to fouling. Equation 29 has been solved for the modified heat transfer coefficient.

$$\frac{1}{A_{fin}h_{foul}} = R_{conv} + R_{foul} = \frac{1}{A_{fin}h} + \frac{R''_{foul}}{A_{fin}} \tag{28}$$

$$h_{foul} = \frac{1}{\frac{1}{h} + R''_{foul}} \tag{29}$$

4.2 Convection and Fin Conduction

Path 1 in Fig. 5 represents heat transfer along the fins and into the fluid. R_1 represents conduction through the joint material underneath the vertical portions of the fin array and R_2 represents conduction through the fin and convection into the fluid. For this portion of the analysis, the folded fin pattern was simplified to rectangular fins with a height H and with an insulated tip. The tops of the fins touch the plenum, but the heat transfer into the plenum was neglected compared to the convection into the fluid along the side of the fin. The characteristic height of a fin, H_c, and area of the fin, A_{fin}, are then defined by Equations 30 and 31. For fin types other than wavy, the value of s_W/P_W is equal to unity. A relation for calculating the fin efficiency, η, for a rectangular fin with an adiabatic tip is given by Incropera et al. (2007) as Equation 32.

$$H_c = H + \frac{\delta_{fin}}{2} \tag{30}$$

$$A_{fin} = 2H_cL\left(\frac{s_W}{P_W}\right) \tag{31}$$

$$\eta = \frac{\tanh\left(\sqrt{\frac{2h_{foul}}{k_{fin}\delta_{fin}}} \cdot H_c\right)}{\sqrt{\frac{2h_{foul}}{k_{fin}\delta_{fin}}} \cdot H_c} \tag{32}$$

The remaining two paths of heat transfer in Fig. 5 are through the gaps between the vertical fins. It was assumed that half the area between fins, A_{base}, is covered as alternating gaps between fins have folded fin material that covers the base. R_3 represents conduction through the joint material underneath the horizontal portions of the fin array, R_4 represents conduction through horizontal portions of the fin material, and R_5 and R_6 represent convection into the fluid. A_{base} was approximated with Equation 33.

$$A_{base} = W \cdot L - N \cdot (L \cdot \delta_{fin}) \left(\frac{S_W}{P_W}\right) \tag{33}$$

The joint between the fins and heat sink was assumed to be a thin layer of bonding material of constant thickness, δ_j, and thermal conductivity, k_j. Following this assumption, the thermal contact resistance of the joint between the fins and base, R_j'', was calculated with Equation 34.

$$R_j'' = \frac{\delta_j}{k_j} \tag{34}$$

The equivalent thermal resistance of all three paths, R_{fin}, is calculated with Equation 35. The flat plate equivalent heat transfer coefficient, h_{eq}, is then given as Equation 36. This value represents the heat transfer coefficient on a flat plate that would be necessary for an equivalent thermal resistance between the coolant and the base.

$$R_{fin} = \frac{1}{\frac{1}{R_1 + R_2} + \frac{1}{R_3 + R_4 + R_5} + \frac{1}{R_6}} \tag{35}$$

$$h_{eq} = \frac{1}{R_{fin} \cdot W \cdot L} \tag{36}$$

4.3 Base Conduction and Spreading Effect

The IGBT modules heat relatively small areas on the underside of the base, and heat is dissipated to the fin structure that covers the entire upper surface. This conduction spreading effect is modeled using a solution to the 3-dimensional steady state heat equation. The domain of Fig. 4 is divided to model one IGBT in an infinite row, as in Fig. 6. The boundary condition for the top of the domain is the equivalent heat transfer coefficient and the coolant inlet temperature. The boundary condition for the footprint of the IGBT is a constant heat flux, q_{in}, equal to one half of the heat generated by the IGBT because the model is for one side of a symmetric system. The IGBT footprints are centered on the domain, but this is not necessary for the solution used. All other faces are insulated.

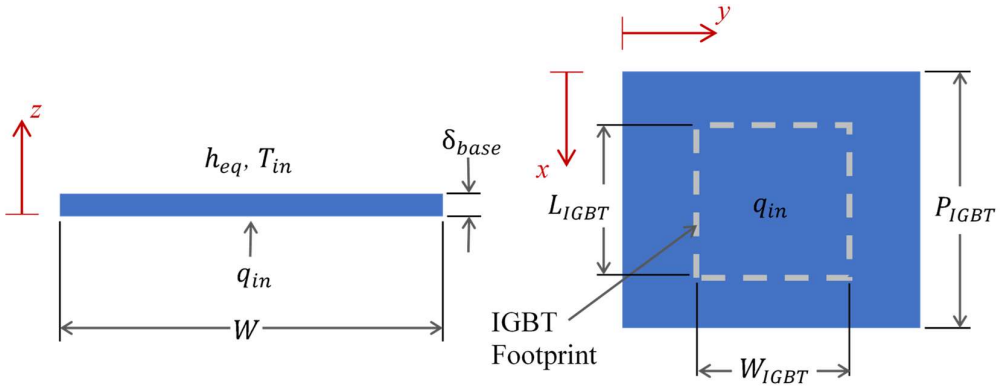

Fig. 6 Base conduction domain: front view (left), bottom view (right).

With these assumptions Ellison (2003) provides the solution to Equation 37 as $T(x, y, z)$, the temperature profile in the domain. The largest observed temperature will be at the center of the footprint of the IGBT, so the solution was solved for $T\left(\frac{P_{IGBT}}{2}, \frac{W}{2}, 0\right)$, given as Equation 38.

$$\frac{\partial^2 T}{\partial x^2}+\frac{\partial^2 T}{\partial y^2}+\frac{\partial^2 T}{\partial z^2}=-\frac{q'''_{gen}}{k_{base}}$$
$$\frac{\partial T}{\partial x}=0 \; at \; x=0, P_{IGBT} \quad \frac{\partial T}{\partial y}=0 \; at \; y=0, W \quad \frac{\partial T}{\partial z}=0 \; at \; z=0 \quad \frac{\partial T}{\partial z}=-h_{eq}T \; at \; z=\delta_{base} \tag{37}$$

$$\mathrm{T}\left(\frac{P_{IGBT}}{2},\frac{W}{2},0\right)=\sum_{l=0}^{n}\sum_{m=0}^{n}\Psi_{lm}\cos\left(\frac{l\pi}{2}\right)\cos\left(\frac{m\pi}{2}\right)+T_{in},$$
$$\text{where } \Psi_{lm}=\left(\frac{16 \;\; in}{\pi^2 lmk_{base}L_{IGBT}W_{IGBT}}\right)\sin\left(\frac{l\pi L_{IGBT}}{2P_{IGBT}}\right)\cos\left(\frac{l\pi}{2}\right)\sin\left(\frac{m\pi W_{IGBT}}{2W}\right)\cos\left(\frac{m\pi}{2}\right)\ldots$$
$$\times\left[\cosh(-\delta_{base}\mathrm{B})-\left(\frac{h_{eq}}{k_{base}\mathrm{B}}\right)\sinh(-\delta_{base}\mathrm{B})\right]\div\left[\mathrm{B}\left(\sinh(\delta_{\mathrm{base}}\mathrm{B})+\left(\frac{h_{eq}}{k_{base}\mathrm{B}}\right)\cosh(\delta_{base}B)\right)\right] \tag{38}$$
$$\text{and } \mathrm{B}=\sqrt{\left(\frac{l\pi}{P_{IGBT}}\right)^2+\left(\frac{m\pi}{W}\right)^2}$$

A convergence test demonstrated that 50 is a sufficient number of Fourier series terms, n, to reach convergence in the solution to four decimal places. Equation 36 is used to calculate R_{base}, the thermal resistance of the base.

$$R_{base}=\frac{T\left(\frac{P_{IGBT}}{2},\frac{W}{2},0\right)-T_{in}}{q_{in}}-R_{fin} \tag{39}$$

4.4 Junction-to-Case and TIM Thermal Resistance

Modeling of heat transfer inside of the IGBT module is beyond the scope of this work, but it is common to reduce the thermal resistance from the IGBT junction to the case to a single value, represented as R_{IGBT}. The thermal resistance of the TIM, R_{TI} , is estimated with Equation 40. The relation for the total junction-to-fluid thermal resistance, R_{tot}, and the junction temperature, T_{junc}, are then given as Equations 41 and 42.

$$R_{TIM}=\frac{\delta_{TIM}}{k_{TIM}W_{IGBT}L_{IGBT}} \tag{40}$$

$$R_{tot}=R_{fin}+R_{base}+R_{TIM}+R_{IGBT} \tag{41}$$

$$T_{junc}=R_{tot}q_{in}+T_{in} \tag{42}$$

5. MODEL DEMONSTRATION AND VALIDATION

5.1 Representative Design Conditions

The model described was applied to conduct trade studies for a folded fin cold plate in a specific application. The prescribed conditions to design a drop-in replacement cold plate for the system are listed in Table 1. Additional constraints were that any fin design could pass a 1 mm particle to reduce the potential for fouling, pressure loss could not exceed 20 kPa, and IGBT junction temperature could not exceed 135 ºC.

5.2 Manufacturability Review

Conducting a meaningful study of the parameters shown in Fig. 2 required defining limits based on manufacturability. A survey was made of limits published by various manufacturers and a conservative summary of the values found is given in Table 2. Additional considerations exist and require discussion with manufacturers to elicit. As a notable example, the specified fin pitch generally must be at least ten times the material thickness to allow for bending bend without fracturing, although this varies with material and temper.

Table 1. Example Design Conditions

Geometry	Value
Flow Length, L	120.5 mm
Plenum Width, W	21.7 mm
Plenum Height, H	5.5 mm
Base Thickness, δ_{base}	2 mm
IGBT Width, W_{IGBT}	12 mm
IGBT Length, L_{IGBT}	12 mm
IGBT Pitch, P_{IGBT}	20.1 mm

Thermal Parameter	Value
Coolant Type	50-50 EG-Water
Coolant Flow Rate, $\dot{V}$	5.0 L/min
Inlet Temperature, T_{in}	75 °C
IGBT Heat, q_{in}	87.5 W
Fouling Factor, R''_{foul}	0 m^2°C/W
$R_{TIM} + R_{IGBT}$	0.15 W/°C

Table 2. Conservative Manufacturing Limits of Folded Fin Geometry*

	Straight Folded Fin		Wavy Folded Fin		Lanced Folded Fin	
Parameter	Max (mm)	Min (mm)	Max (mm)	Min (mm)	Max (mm)	Min (mm)
Flow Length, L	610	3.18	610	3.18	508	9.53
Flow Width, W	*none*	0	*none*	0	*none*	0
Fin Height, H	50.8	5.08	101.6	5.08	19.0	9.14
Fin Pitch, P_{fin}	25.4	0.591	25.4	0.782	25.4	1.27
Material Thickness, δ_{fin}	2.03	0.0508	1.02	0.0508	0.508	0.0508
Wave Height, H_W			2.54	0.254		
Wave Pitch, P_W			38.1	3.175		
Lance Length, L_L					25.4	2.54
Lance Offset					6.35	0.318

*Niagara Thermal Products (2011), Aavid Thermalloy (2012), Robinson Fin (1997, 2004, 2011), Tucker Engineering (2011)

5.3 Material Properties

Assuming constant material properties at a known temperature avoids an iterative solution process. Later numerical analysis predicted temperature extremes across the domain corresponding to deviations of less than 1% in all material properties from assumed values. Properties of the coolant were evaluated at the inlet temperature of 75°C as listed in Table 3. The solid materials considered were aluminum (UNS A96061) and copper (UNS C11000) because of cost, thermal performance, and compatibility with the system. Properties in Table 4 were evaluated at 100 °C. Properties of the bonding materials are tabulated in Table 5. Thickness, δ_j, was approximated as 0.05 mm for a brazed or soldered joint and 0.1 mm for epoxy. Dissimilar fin and base materials can be used, with additional engineering considerations such as galvanic corrosion. For a brazed joint the thermal conductivity, k_j, was approximated as average of the two materials. For solder k_j was approximated as 40 W/m°C and for epoxy k_j was approximated as 1 W/m°C (Lou et al., 2000).

Table 3. Properties of 50%-50% Ethylene Glycol and Water at 75°C (ASHRAE, 2009)

Density $\left(\frac{kg}{m^3}\right)$	Absolute Viscosity, μ $\left(\frac{N \cdot s}{m^2}\right)$	Thermal Conductivity, k $\left(\frac{W}{m \cdot °C}\right)$	Specific Heat c_p $\left(\frac{J}{kg \cdot °C}\right)$	Prandtl Number, Pr (-)
1042.04	0.00107	0.392	3490	9.53

Table 4. Properties of Copper and 6061 Aluminum at 100 °C (Mills, 2002)

Material	Density, ρ $\left(\frac{\text{kg}}{\text{m}^3}\right)$	Specific Heat, c $\left(\frac{\text{J}}{\text{kg} \cdot {}^{\text{o}}\text{C}}\right)$	Thermal Conductivity, k $\left(\frac{\text{W}}{\text{m} \cdot {}^{\text{o}}\text{C}}\right)$
Copper	8890	397	395
Aluminum 6061	2695	950	195

Table 5. Contact Thermal Resistance Data

Joint Type	t_j (mm)	k_j $\left(\frac{\text{W}}{\text{m} \cdot {}^{\text{o}}\text{C}}\right)$	R_j'' $\left(\frac{\text{m}^2 \cdot {}^{\text{o}}\text{C}}{\text{W}} \cdot 10^6\right)$
Brazed (Cu-Cu)	0.05	395	0.127
Brazed (Cu-Al)	0.05	295	0.169
Brazed (Al-Al)	0.05	195	0.256
Solder	0.05	40	1.25
Epoxy	0.1	1	100

5.4 Trade Study

A trade study was conducted of designs with combinations of straight, wavy, and lanced fins; copper and aluminum fins and base; and brazed, soldered and epoxy joints. Each was evaluated at hundreds of combinations of the geometric parameters not specified in Table 1, within the limits of Table 2. The solution speed of this analytic model allows for a brute-force search along many dimensions, generating thousands of data points. For a subset of the designs, pressure loss and predicted IGBT junction temperature are plotted in Fig. 7.

Folded fin heat sinks generally have low blocking ratio, β, due to the relatively thin material stock and wide fin pitch required to bend material without fracture. As a result, all designs meet the maximum pressure loss requirement. The wavy fin designs had the best thermal performance. The lanced folded fins designs performed more poorly under this system's design constraints due to the required fin pitch being larger in a lanced fin design in order to pass a 1 mm particle. A final observation was that none of the epoxied designs met the maximum junction temperature criteria of 135 °C, and are therefore absent from Fig. 7.

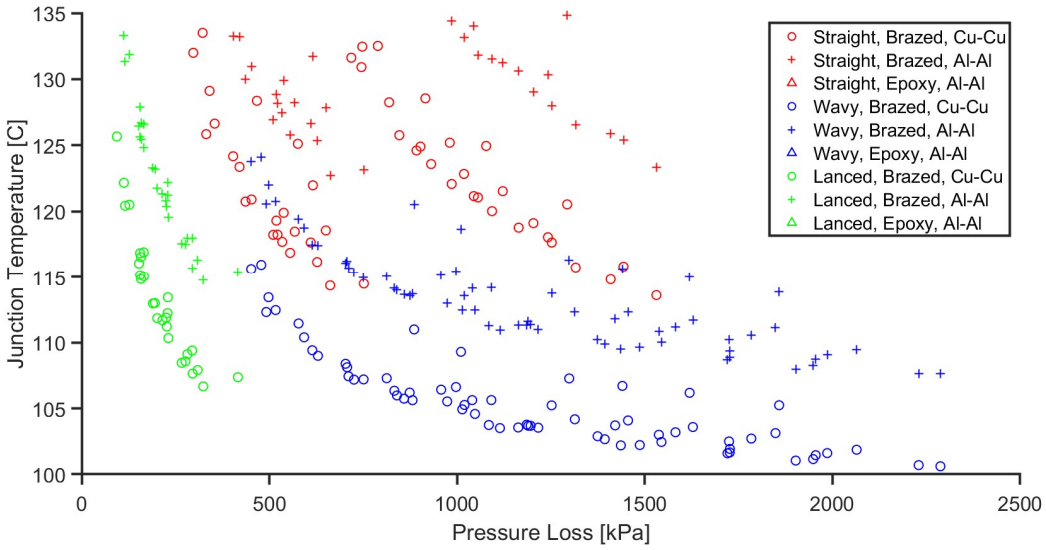

Fig. 7 Subset of data from a trade study of various folded fins designs.

5.5 Wavy Folded Fin Cold Plate Design

A wavy folded fin cold plate was selected for further study due to better thermal performance than the other fin types. A prototype design was developed based on the best performing designs from Fig. 7 and a manufacturer's existing tooling. A preferred design was selected with the same corrugation ratio but a shorter wave pitch. It is known that wavy channels produce increased turbulence several periods downstream from the channel entrance (Rush et al., 1999). A shorter wave pitch produces turbulence closer to the leading edge of the cold plate, increasing cooling of the first few IGBTs. The geometries of both designs are shown in Fig. 8 and Table 6.

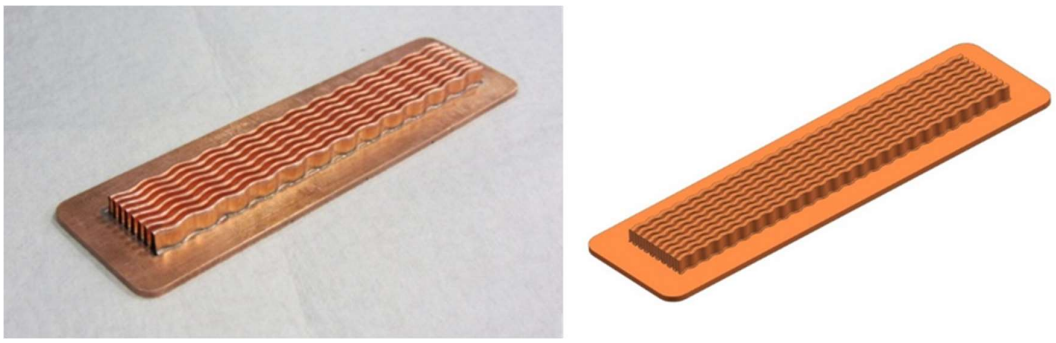

Fig. 8 Prototype (left) and preferred (right) folded fin cold plate designs.

Table 6. Geometry of Folded Fin Cold Plate Designs

Prototype Cold Plate Geometric Parameter	Value (mm)
Fin Pitch, P_{fin}	2.406
Material Thickness, δ_{fin}	0.203
Wave Height, H_W	1.3
Wave Pitch, P_W	9.5

Preferred Cold Plate Geometric Parameter	Value (mm)
Fin Pitch, P_{fin}	2.406
Material Thickness, δ_{fin}	0.203
Wave Height, H_W	0.65
Wave Pitch, P_W	4.75

5.6 Numerical Validation

3D numerical models of the Fig. 8 designs were analyzed with a commercial CFD software package, FLUENT. Due to computational limitations, solid and fluid domains were uncoupled as in Fig. 9. The total solid-fluid interface area, A_{tot}, was calculated and used to determine a heat flux, q''_{in}, as a boundary condition for the fluid domain. The average heat transfer coefficient from the fluid domain was then applied to the solid domain as a boundary condition. A more accurate layout of the IGBT footprint was modeled with $q_{in,IGBT}$ of 87.5 W. In addition, the model included a 21 W heat load from each diode, $q_{in,diod}$, that could not be modeled analytically. All boundaries not described were treated as no-slip, no-penetration, insulated boundaries.

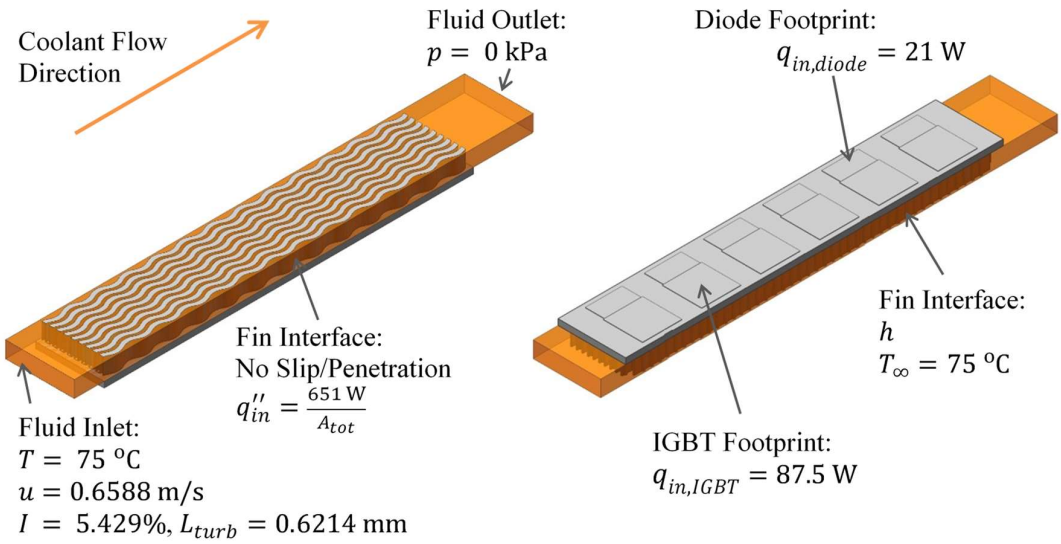

Fig. 9 Domain of the 3D numerical model of the folded fin cold plates: fluid boundary conditions (left), solid boundary conditions (right).

An unstructured tetrahedral mesh was generated in the ANSYS meshing tool. A maximum first cell height corresponding to $y^+ = 5$ was specified, as recommended by Fluent, Inc. (2007), along with a maximum growth ratio and a maximum cell size that were controlled to refine the mesh. A smoothing operation was required to reduce the maximum cell skewness to below 0.9, increasing average cell skewness which remained below 0.3. A pressure-based solver was used with second order upwind spatial discretization and the pressure-implicit with splitting of operators (PISO) algorithm for pressure-velocity coupling, as recommended by Fluent, Inc. (2007) for high-skew meshes. Turbulence was modeled with the realizable $k-\epsilon$ model with enhanced wall functions. Initial turbulence parameters, I and L_{turb}, were calculated for steady flow in a duct equivalent to the plenum without any fins. The model described was used to predict performance for the prototype and preferred folded fin cold plate designs, shown in Table 7. Estimated performance for a proprietary, more exotic cold plate design currently in use is presented as a benchmark.

Table 7. Performance Estimate Comparison for the Analytic Model and Numerical Model

Model	Cold Plate Design	Δp kPa	h $\frac{\text{W}}{\text{m}^2 \cdot {}^\circ\text{C}}$	R_{tot} $\frac{{}^\circ\text{C}}{\text{W}}$	T_{junc} °C
Analytic	Prototype (Cu-Cu)	2.154	5295	0.3014	101.4
	Preferred (Cu-Cu)	2.659	7487	0.2822	99.7
	Preferred (Al-Al)	2.659	7487	0.3574	106.3
Numerical	Prototype (Cu-Cu)	4.438	7102	0.2949	100.8
	Preferred (Cu-Cu)	6.051	8445	0.2846	99.9
	Preferred (Al-Al)	6.051	8445	0.3520	105.8
Numerical	Legacy Design (Proprietary)	19.50	12930	0.2777	99.3

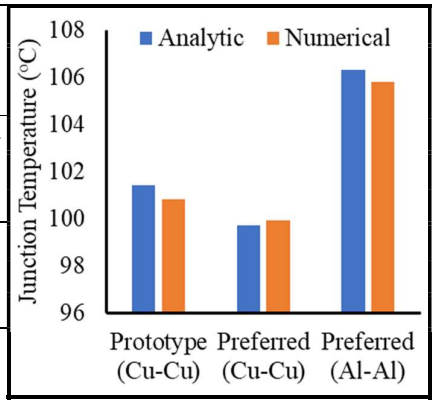

6. SUMMARY AND CONCLUSIONS

The results given in Table 7 demonstrated excellent agreement between models. Despite uncertainty in the empirical flow correlations, various geometric simplifications, and exclusion of the diode heat source, the calculation of an accurate junction temperature prediction is possible with an analytic model. For the wavy fin design, the worst-case RMS error reported for the empirical flow correlations used was as high as 50%. However,

a change of +/- 50% in the value for h will produce a change in estimated junction temperature of less than 5 ^{o}C. The pressure loss estimates showed less agreement with the numerical model. However, the pressure loss was far less than the legacy design and pressure loss is less likely to be a limiting factor with folded fins due to the inherently low blocking ratio.

The model presented allows for fast trade studies, with the solution time to generate Fig. 7 at less than one minute on a consumer-grade laptop. Implementation of the model in the programming language MATLAB required less than 150 lines of code. Multiple runs of the model are simple to setup in a programming language or a spreadsheet software. This capability greatly complements the use of numerical analysis in industry and academic studies. The analytic model can also be used to verify solutions from numerical analysis with greater confidence than the oversimplified by-hand methods commonly used for validation.

The details of the model presented are specific to three types of folded fin cold plate design. However, the model can be expanded to other types of folded fins if empirical flow correlations are available. For cold plate designs that don't use folded fins, most of the methods described are still applicable and would be useful for design work.

This work demonstrates the potential of low-cost fin solutions, particularly the folded fin, to provide thermal performance comparable to more expensive designs. Despite a significantly higher convective heat transfer coefficient, a proprietary design currently in use does not provide significant reduction in junction temperature due to dominance of other thermal resistances, such as the junction-to-case thermal resistance of the IGBT package and the thermal resistance of the TIM.

ACKNOWLEDGMENT

The authors acknowledge the support of Delphi Electronics & Safety.

NOMENCLATURE

English Symbols		
I	turbulence intensity	$(-)$
j	Colburn factor	$(-)$
n	number of Fourier terms	$(-)$
N	number of fins/channels	$(-)$
P	pitch	(mm)
R	thermal resistance	(^{o}C/W)

Greek Symbols		
α	channel aspect ratio	$(-)$
β	fin blocking ratio	$(-)$
γ	corrugation ratio	$(-)$
η	fin efficiency	$(-)$

Subscripts	
app	apparent
avg	average
base	base of the cold plate
c	characteristic
conv	convection
chan	coolant channel
diode	for the diode
eq	equivalent
equation	from equation X
fin	fins of the cold plate
foul	fouled surface
IGBT	for the IGBT
j	fin-to-base joint
junc	for the IGBT junction
L	for lanced folded fins
LBL	laminar boundary layer
W	for wavy folded fins
wet	wetted interface
TIM	interface material
tot	total
turb	turbulence

REFERENCE LIST

[1] Awad, M.M. and Muzychka, Y.S., "Models for pressure drop and heat transfer in air cooled compact wavy fin heat exchangers," *Journal of Enhanced Heat Transfer,* 18(3), pp. 191-207, (2011).

[2] Kim, M., Lee, J., Yook S., Lee, K., "Correlations and optimization of a heat exchanger with offset-strip fins," *Int. J. Heat Mass Transf.*, 54(9-10), pp. 2073-2079, (2011).

[3] Shah, R.K. and London, A.L., *Laminar Flow Forced Convection in Ducts*, New York: Academic Press, pp. 196-222 (1978).

[4] Petukhov, B.S., "Heat Transfer and Friction in Turbulent Pipe Flow with Variable Physical Properties," In J. P. Hartnett and T.F. Irvine Jr., Eds., *Advances in Heat Transfer*, New York: Academic Press, pp. 503-564 (1970).

[5] Gnielinksi, V. "New equations for heat and mass transfer in turbulent pipe and channel flow," *Int. J. of Chem. Eng.,*16(2), pp. 359-368, (1976).

[6] Sheik Ismail, L., Velraj, R., Ranganayakulu, C., "Studies on pumping power in terms of pressure drop and heat transfer characteristics of compact plate-fin heat exchangers—A review," *Renewable Sustainable Energy Rev,* 14(1), pp 478-485, (2010).

[7] Aliabadi, M.K., Hormozi, F., Rad, E.H. "New correlations for wavy plate-fin heat exchangers: different working fluids," *Int. J. Numer. Methods Heat Fluid Flow*, 24(5), pp. 1086-1108, (2014).
[8] Kurtulmus, N. and Sahin, B., "A review of hydrodynamics and heat transfer through corrugated channels," *Int. Commun. Heat Mass Transf.*, 108, (2019)
[9] Sparrow, E.M. and Hossfeld, L.M., "Effects of rounding of protruding edges on heat transfer and pressure drop in a duct," *Int. J. Heat Mass Transf.*, 27(10), pp. 1715-1723, (1984).
[10] Gradeck, M., Hoareau, B., Lebouche, M., "Local analysis of heat transfer inside corrugated channel," *Int. J. Heat Mass Transf.*, 48(10), pp. 1909-1915, (2005).
[11] Junqi, D., Jiangping, C., Zhijiu, C., Yimin, Z., Wenfeng, Z., "Heat transfer and pressure drop correlations for the wavy fin and flat tube heat exchangers," *Appl. Therm. Eng.* 27(11-12), pp. 2066-2073, (2007).
[12] Shapiro, A.H., Siegel, R., Kline, S.L., "Friction factor in the laminar entry region of a smooth tube," *Proc. 2nd. Natl. Congr. Appl. Mech.*, pp. 733-741, (1954).
[13] Joshi, H.M. and Webb, R.L. "Heat transfer and friction in the offset stripfin heat exchanger," *Int. J. Heat Mass Transf*, 30(1), pp. 69-84, (1987).
[14] Manglik, R.M. and Bergles, A.E., "Heat transfer and pressure drop correlations for the rectangular offest strip fin compact heat exchanger," *Exp. Therm. Fluid Sci.*, 10(2), pp. 171-180, (1995).
[15] Incropera, F.P., DeWitt, D.P., Bergman, T.L., Lavine, A.S., *Introduction to Heat Transfer*, Hoboken, NJ: John Wiley & Sons, pp. 137-162, (2007).
[16] Ellison, G.N., "Maximum thermal spreading resistance for rectangular sources and plates with nonunity aspect ratios," *IEEE Trans. Compon. Packag. Technol.*, 26(2), pp. 439-454, (2003).
[17] Niagara Thermal Products, *Custom Heat Transfer Fin*. Retrieved June 10, 2011 from http://heatexchangers.niagarathermal.com/item/all-categories/custom-heat-transfer-fin/item-1016?#.
[18] Aavid Thermalloy, *Folded Fin Assemblies.* Retrieved April 9, 2012 from https://www.aavidthermalloy.com/product-group/foldedfin.
[19] Robinson Fin, *Plain Fin Terminology for Robinson Fin*. Retrieved June 6, 2011 from http://www.robfin.com/portals/0/R600002%20plain%20Model%20(1).pdf, (2004)
[20] Robinson Fin, *Ruffled Fin Terminology for Robinson Fin*. Retrieved June 6, 2011 from http://www.robfin.com/portals/0/R600006%20ruffled%20Model%20(1).pdf.
[21] Robinson Fin, *Lanced Fin Terminology for Robinson Fin*. Retrieved June 6, 2011 from http://www.robfin.com/portals/0/R600003%20lanced%20Model%20(1).pdf, (1997).
[22] Tucker Engineering, *Folded Fin Heatsinks*. Retrieved June 6, 2011 from http://www.tuckereng.com/folded-fin.htm.
[23] Loh, C.K., Chou, B., Nelson, D., Chou, D.J., "Study of Thermal Characteristics on Solder and Adhesive Bonded Folded Fin Heat Sink," *Proc. 7th Intersociety Conf. Therm. Thermomechanical Phenom. In Electron. Syst.,* 00CH37069, 2, pp. 1-7, (2000).
[24] American Society of Heating, Refrigerating, and Air-Conditioning Engineers, *2009 ASHRAE Handbook - Fundamentals*, Atlanta: ASHRAE, pp. 31.7-31.8, (2009).
[25] Mills, K.C., *Recommended Values of Thermophysical Properties for Selected Commercial Alloys*, Cambridge: Woodhead Publishing, pp.19-104, (2002).
[26] Rush, T.A., Newell, T.A., Jacobi, A.M., "An experimental study of flow and heat transfer in sinusoidal wavy passages," *Int. J. Heat Mass Transf*, vol. 42(9), pp. 1541-1553, (1999).
[27] Fluent Inc., *FLUENT 6.3 Documentation*, [Online]. Retrieved June 20, 2011 from http://hpce.iitm.ac.in/website/Manuals/Fluent_6.3/fluent6.3/help/index.htm, (2007).